

Analytic quantization of the QCD string

Theodore J. Allen

Physics Department, Hobart & William Smith Colleges, Geneva, New York 14456

Charles Goebel and M. G. Olsson

Department of Physics, University of Wisconsin, 1150 University Avenue, Madison, Wisconsin 53706

Siniša Veseli

Fermi National Accelerator Laboratory, P. O. Box 500, Batavia, Illinois 60510

(Received 15 June 2001; published 4 October 2001)

We perform an analytic semiclassical quantization of the straight QCD string with one end fixed and a massless quark on the other, in the limits of orbital and radial dominant motion. We compare our results to the exact numerical semiclassical quantization. We observe that the numerical semiclassical quantization agrees well with our exact numerical canonical quantization.

DOI: 10.1103/PhysRevD.64.094011

PACS number(s): 12.38.Aw

I. INTRODUCTION

The purpose of this paper is to explore some remarkable results of the QCD string or flux tube model [1–3]. In its relativistic and single quantized form [3] a particularly simple pattern emerges when one or both quarks are light. For the purposes of this paper we take the light quarks to have zero mass. In this case the energy E of the light degrees of freedom (LDF's) and the angular and radial quantum numbers (J and n respectively) are accurately related by

$$\frac{E^2}{(2)\pi a} \approx J + 2n + \frac{3}{2} \quad (1.1)$$

for one (or two) light quark(s). For the case of one light quark the meson energy is the sum of E and the heavy quark mass.

The above pattern of angular and radial states results in degenerate “towers” of mesons of the same parity. This is the same pattern as the 3D harmonic oscillator.

The QCD string model is kinematically intricate and it would seem unlikely that it would lead to such a simple result as Eq. (1.1). We demonstrate in this paper that although Eq. (1.1) is not exact, it is very accurate for most accessible quantum states. The quantized relativistic flux tube model is of great interest because of the probability that QCD reduces to string-like behavior at large source separations [4].

The simplest version of a quark string model assumes that the string is always straight. In the limiting cases of circular motion or pure radial motion this assumption is physically reasonable. In addition, for massive quarks at the ends the relativistic corrections have been shown [5] to agree with the Wilson loop description of QCD confinement [6]. Numerical quantization of the straight string and quark system has been done canonically [3] with the Nambu-Goto string, as well as in the WKB approximation with an auxiliary field method [7]. Both approaches give results similar to Eq. (1.1).

More generally, one may allow the string to curve adiabatically by incorporating the string equations of motion

from the Nambu-Goto action [8]. This more general string calculation demonstrates that the string curvature remains small for motion in ordinary hadrons. The string curvature only slightly changes the energies of the bound states, justifying the use of the simpler straight string approximation.

The approach emphasized here is to quantize the straight string system semiclassically. We will show that this quantization agrees well with our previous exact quantization method. We will also show that a single integral function then predicts the whole spectroscopy when at least one quark is massless. We will approximate this integral analytically in sectors when $J \gg n$ and when $n \gg J$. The latter case where radial motion dominates is valid over most of the allowed bound states.

II. DYNAMICS AND QUANTIZATION

A. Dynamics

As we mentioned earlier, the straight QCD string is an excellent approximation to the dynamical (curved) string in normal hadrons. We will therefore restrict ourselves to the relatively simple straight string. We will explicitly consider the case of one fixed end and a quark of mass m at the other. The string with two light quarks introduces only minor modifications, which we discuss at the end of Sec. II. As is well known [3], the two constants of motion are the orbital angular momentum J and the energy E of the light degrees of freedom, which are given in terms of the quark's transverse velocity v_\perp and radial momentum p_r as

$$J = W_r \gamma_\perp v_\perp r + ar^2 f(v_\perp), \quad (2.1)$$

$$E = W_r \gamma_\perp + arS(v_\perp), \quad (2.2)$$

where $W_r = \sqrt{p_r^2 + m^2}$, $\gamma_\perp = (1 - v_\perp^2)^{-1/2}$, r is the string length, and a is the string tension. The functions f and S that appear in the expressions for the angular momentum and energy are

$$f(v_{\perp}) = \frac{1}{2v_{\perp}} (S(v_{\perp}) - \sqrt{1-v_{\perp}^2}), \quad (2.3)$$

$$S(v_{\perp}) = \frac{\sin^{-1}(v_{\perp})}{v_{\perp}}. \quad (2.4)$$

For our present purposes we will introduce a set of dimensionless variables. As our units we take the circular orbit radius (in the limit of a massless quark)

$$r_0 = 2 \sqrt{\frac{J}{\pi a}}, \quad (2.5)$$

and corresponding string energy

$$E_0 = \sqrt{J\pi a}. \quad (2.6)$$

Our dimensionless variables Δ , ρ , and w are defined by

$$\frac{E}{E_0} \equiv \sqrt{1+\Delta^2}, \quad (2.7)$$

$$\frac{r}{r_0} \equiv \sqrt{1+\Delta^2} + \rho\Delta, \quad (2.8)$$

and

$$w \equiv \frac{W_r}{E_0}. \quad (2.9)$$

The leading (classical) Regge trajectory corresponds to $\Delta = 0$ and radial excitation occurs for positive Δ .

In terms of these dimensionless variables the conserved quantities (2.1) and (2.2) become

$$1 = 2w\gamma_{\perp}v_{\perp}[\sqrt{1+\Delta^2} + \rho\Delta] + \frac{4}{\pi}f(v_{\perp})[\sqrt{1+\Delta^2} + \rho\Delta]^2, \quad (2.10)$$

$$\sqrt{1+\Delta^2} = w\gamma_{\perp} + \frac{2}{\pi}S(v_{\perp})[\sqrt{1+\Delta^2} + \rho\Delta]. \quad (2.11)$$

After some work, we can eliminate the product $w\gamma_{\perp}$ to obtain

$$2v_{\perp}[\sqrt{1+\Delta^2} + \rho\Delta]\sqrt{1+\Delta^2} - \frac{4}{\pi}(v_{\perp}S(v_{\perp}) - f(v_{\perp}))[\sqrt{1+\Delta^2} + \rho\Delta]^2 = 1 \quad (2.12)$$

and rewrite Eq. (2.11) to find an expression for w :

$$w = \sqrt{1-v_{\perp}^2} \left[\sqrt{1+\Delta^2} - \frac{2}{\pi}S(v_{\perp})(\sqrt{1+\Delta^2} + \rho\Delta) \right]. \quad (2.13)$$

At the radial turning points $p_r = 0$. The radial velocity also vanishes, except in the massless quark limit.

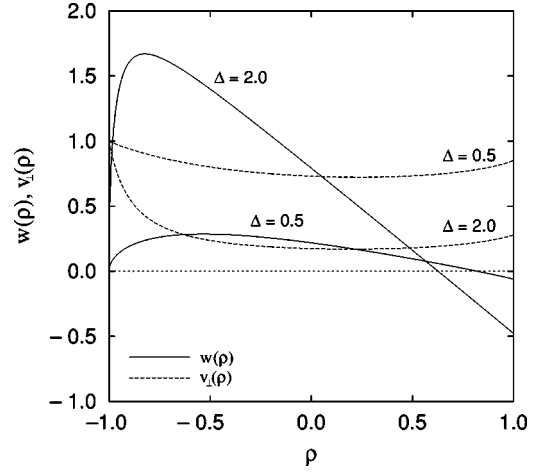


FIG. 1. Exact numerical solutions of Eq. (2.12) and Eq. (2.13) for $w(\rho)$ and $v_{\perp}(\rho)$ for the values $\Delta=0.5$ and $\Delta=2.0$.

The reason for the definition of the radial coordinate ρ in Eq. (2.8) will be evident in this limit. If we take the limit $v_{\perp} = 1$ this will correspond to $\dot{r} = 0$ in the massless quark case. Using $f(1) = \pi/4$ and $S(1) = \pi/2$ in Eq. (2.12) we see that the solution is $\rho^2 = 1$ for any Δ . The points $\rho = \pm 1$ therefore correspond to possible turning points.

By Eq. (2.13) we see that at $v_{\perp} = 1$, $w = 0$. This would seem to be the expected result in the massless quark case. However, as we see in Fig. 1, the second factor in Eq. (2.13) has a zero at $\rho < 1$ and is the true turning point. In Fig. 1 we show representative numerical solutions with $\Delta = 0.5$ and $\Delta = 2.0$. First we solve Eq. (2.12) for v_{\perp} for $-1 < \rho < +1$ and substitute into Eq. (2.13) to compute $w(\rho)$. The turning points of the general motion are $\rho_- = -1$ and $\rho_+ < 1$. We will show later that in the massless quark case

$$\frac{\pi}{2} - 1 \leq \rho_+ \leq 1, \quad (2.14)$$

where the lower limit is achieved for large Δ and $\rho_+ = 1$ when $\Delta = 0$.

The outer turning point in the massless case is a ‘‘bounce’’ where \dot{r} discontinuously changes sign.

B. Quantization

The semi-classical quantization condition for a spherically symmetric system is [9]

$$\int_{r_-}^{r_+} dr p_r(r, J+1/2) = \pi \left(n + \frac{1}{2} \right), \quad (2.15)$$

where $n = 0, 1, 2, \dots$ and it is understood that the Langer correction [9,10] replaces the classical angular momentum J by $J+1/2$, where J is now the angular momentum quantum number. In terms of our dimensionless parameters ρ and w , the above quantization condition becomes

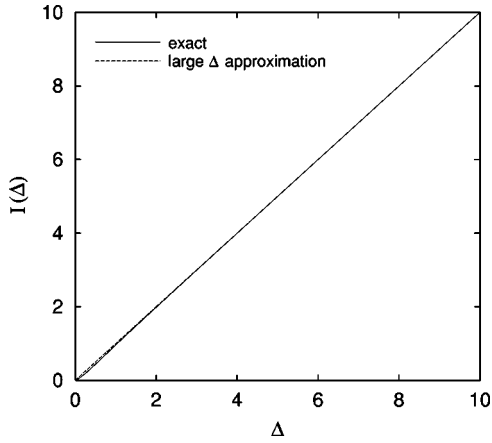


FIG. 2. A comparison of the exact numerical solution of Eq. (2.17) for $I(\Delta)$ with the leading order approximation $I(\Delta) \simeq \Delta$.

$$\frac{4}{\pi} \int_{-1}^{\rho_+} d\rho \sqrt{w^2 - \frac{m^2}{\left(J + \frac{1}{2}\right) a \pi}} = \frac{(2n+1)}{\left(J + \frac{1}{2}\right) \Delta}. \quad (2.16)$$

For our purposes, the massless quark will be of central interest. In this case, there is no J dependence on the left hand side of Eq. (2.16) and, by defining

$$I(\Delta) = \frac{4}{\pi} \int_{-1}^{\rho_+} d\rho w(\rho), \quad (2.17)$$

we obtain

$$\Delta I(\Delta) = \frac{2n+1}{J + \frac{1}{2}}. \quad (2.18)$$

The remarkable aspect of the massless quantization condition is that the whole spectrum is revealed once $I(\Delta)$ is computed. In Fig. 2, we show the numerical result of this integration. For a given Δ and ρ we use Eq. (2.12) to find v_{\perp} . The result is used in Eq. (2.13) to find $w(\rho)$. This is then used in Eq. (2.17) to compute $I(\Delta)$. The upper integration limit is determined by the zero in $w(\rho)$, as shown in Fig. 1.

It is evident from Fig. 2 that $I(\Delta)$ is essentially linear in Δ with unit slope. The LDF energy dependence is related to Δ by Eq. (2.7):

$$\Delta = \left[\frac{E^2}{\left(J + \frac{1}{2}\right) a \pi} - 1 \right]^{1/2}, \quad (2.19)$$

where we have again used the Langer correction to the angular momentum. Using the quantization condition, Eq. (2.18), we can map out the entire Regge structure as shown by the curves in Fig. 3. The trajectories are labeled by different radial excitations $n=0,1,2,\dots$. The $n=0$ trajectory is normally called the “leading trajectory” and the $n>0$ trajectories are known as the “daughter trajectories.” The solid points are the exact numerical solutions by the exact canonical

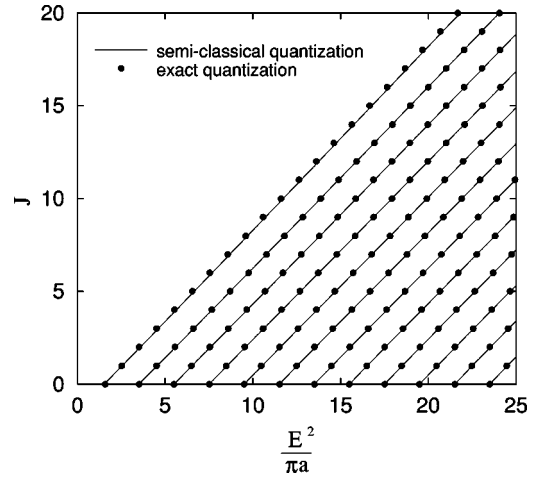


FIG. 3. The Regge trajectories from the semiclassical analysis (lines) and by numerical canonical quantization (dots).

quantization method [3]. The nearly perfect agreement between the semiclassical and canonical quantization should be noted. It is only along the leading trajectory that small differences arise. If there are differences, this is where they should appear since the semiclassical quantization becomes exact for large radial excitation where the wave function has many nodes.

Figure 2 shows that for $\Delta > 1$, $I(\Delta)$ is essentially equal to Δ . In general we expect an expansion in Δ^{-1} to have odd powers of the form

$$I(\Delta) \xrightarrow{\Delta \gg 1} \Delta + \frac{c}{\Delta} + \dots \quad (2.20)$$

A detailed examination of our exact numerical integration of Eq. (2.17) shows that

$$c \simeq -0.006. \quad (2.21)$$

The small magnitude of the coefficient c reflects the extraordinary accuracy of $I(\Delta) = \Delta$ for large Δ .

The string with two light quarks can be considered as two single light quark strings with their fixed ends coinciding at the center of mass point. The resulting light meson equations following from Eqs. (2.1) and (2.2) are

$$J_L = W_r \gamma_{\perp} v_{\perp} r_L + \frac{1}{2} a r_L^2 f(v_{\perp}), \quad (2.22)$$

$$E_L = 2W_r \gamma_{\perp} + a r_L S(v_{\perp}), \quad (2.23)$$

where $r_L = 2r$, $J_L = 2J$, and $E_L = 2E$.

We recover Eq. (2.12) upon rescaling:

$$E_{0L} = \sqrt{2\pi a} J_L, \quad (2.24)$$

$$J_{0L} = 2 \sqrt{\frac{2J_L}{a\pi}}. \quad (2.25)$$

Using Eq. (2.13), we may now identify

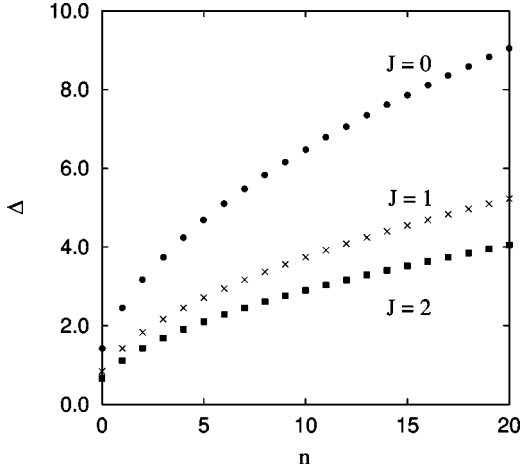


FIG. 4. The dependence of Δ upon the radial quantum number n and the angular momentum quantum number J . Increasing n leads to increasing Δ .

$$W_r \equiv \frac{1}{2} \sqrt{2\pi a J_L} w(\rho), \quad (2.26)$$

and the quantization condition with $I(\Delta) \approx \Delta$ yields

$$\frac{E_L^2}{2\pi a} = J_L + 2n + \frac{3}{2}, \quad (2.27)$$

in agreement with Eq. (1.1).

III. RADIAL DOMINANCE ANALYTIC SOLUTION

A. Leading order

As verified by examining Fig. 4, large n corresponds to large Δ since at fixed angular momentum, both make the LDF energy E increase without bound. By examining Eq. (2.12), we see that for large Δ either $\rho = -1$ or v_\perp is small. To verify this we note that

$$v_\perp S(v_\perp) - f(v_\perp) = 2v_\perp/3 + O(v_\perp^3). \quad (3.1)$$

Hence, except at $\rho = -1$, $v_\perp \ll 1$ in the $\Delta \gg 1$ limit.

In the vanishing v_\perp limit the expression (2.13) for $w(\rho)$ then becomes

$$w(\rho) \rightarrow \Delta \left[1 - \frac{2}{\pi} (1 + \rho) \right]. \quad (3.2)$$

We note that the zero in w that follows from Eq. (3.2) is

$$\rho_+ = \frac{\pi}{2} - 1. \quad (3.3)$$

In Fig. 5 we show the exact numerical result (solid curve) as well as the large Δ approximation (LO) for $\Delta = 2$.

In this regime we may analytically evaluate the quantization integral $I(\Delta)$ in Eq. (2.17) to be

$$I(\Delta) = \Delta. \quad (3.4)$$

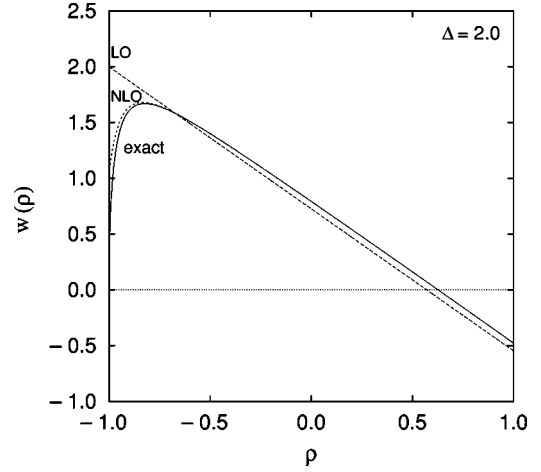


FIG. 5. A comparison of the exact numerical solution of Eq. (2.13) for $w(\rho)$ (lowest curve) with the leading order solution Eq. (3.2) (highest curve) and the solution to next to leading order, Eq. (3.10) (intermediate curve).

Substitution of this into Eq. (2.18) with the use of Eq. (2.19) quickly yields

$$\frac{E^2}{\pi a} = J + 2n + \frac{3}{2}. \quad (3.5)$$

This is a good representation of the massless quark spectroscopy, as we will discuss in the conclusion, Sec. V. This is a reflection of the agreement of the asymptotic (large Δ) values of $I(\Delta)$ down to small Δ .

Finally, we note that the spectrum in Eq. (3.5) is very similar to the three dimensional harmonic oscillator spectrum as we have pointed out previously in the context of the Lorentz scalar confinement of massless quarks.

B. Corrections to leading order

Although in leading order in Δ the result $I(\Delta) = \Delta$ is very accurate, the distribution $w(\rho)$ computed to the same approximation is not as satisfactory, as can be seen in Fig. 5. In this section we attempt to obtain a somewhat better approximation to these two quantities.

Using Eq. (2.12) and the limiting behavior of Eq. (3.1), we find the dependence of v_\perp on ρ and Δ :

$$v_\perp = \left[2(\sqrt{1 + \Delta^2} + \rho\Delta) \left(\sqrt{1 + \Delta^2} - \frac{4}{3\pi}(\sqrt{1 + \Delta^2} + \rho\Delta) \right) \right]^{-1}. \quad (3.6)$$

The value for the upper turning point coordinate ρ_+ can be found from the vanishing of Eq. (2.13) for small v_\perp , which yields

$$\rho_+ = \frac{\sqrt{1 + \Delta^2}}{\Delta} \left(\frac{\pi}{2} - 1 \right). \quad (3.7)$$

With this value of ρ_+ , Eq. (3.6) determines the value of v_\perp at the upper turning point:

$$v_{\perp}^{+} = \left(\frac{3}{\pi}\right) \frac{1}{1+\Delta^2}. \quad (3.8)$$

To second order in v_{\perp} , $w(\rho)$ becomes

$$w \simeq \sqrt{1+\Delta^2} \left(1 - \frac{2}{\pi}\right) - \frac{2\rho\Delta}{\pi} - \frac{v_{\perp}^2}{2} \left[\sqrt{1+\Delta^2} - \frac{4}{3\pi} (\sqrt{1+\Delta^2} + \rho\Delta) \right]. \quad (3.9)$$

Upon substitution of the result of Eq. (3.6), $w(\rho)$ becomes

$$w \simeq \sqrt{1+\Delta^2} \left(1 - \frac{2}{\pi}\right) - \frac{2\rho\Delta}{\pi} - \frac{[\sqrt{1+\Delta^2} - \rho\Delta]^2}{8[\sqrt{1+\Delta^2} - (4/3\pi)(\sqrt{1+\Delta^2} + \rho\Delta)]} \equiv w_1 + w_2, \quad (3.10)$$

with w_1 being the piece of Eq. (3.9) that is finite in the limit of vanishing v_{\perp} . The next-to-leading-order result is shown in Fig. 5. We see that it comes much closer to the exact $w(\rho)$ but deviates slightly near $\rho = -1$ where the small v_{\perp} expansion fails.

It is not difficult to evaluate the integral in Eq. (2.17) by changing the integration variable from ρ to

$$x \equiv \sqrt{1+\Delta^2} + \rho\Delta. \quad (3.11)$$

Splitting $I(\Delta) = I_1(\Delta) + I_2(\Delta)$ according to Eq. (3.10), we find

$$I_1(\Delta) = \frac{1}{\Delta} \left(\frac{2}{\pi}\right)^2 \left[\left(\frac{\pi}{2} - 1\right) \sqrt{1+\Delta^2} + \Delta \right]^2, \quad (3.12)$$

$$I_2(\Delta) = \frac{1}{2\pi\Delta(1+\Delta^2)} \left[\frac{2}{\pi} - 1 - \Delta^2 - \Delta \sqrt{1+\Delta^2} - \frac{4}{3\pi} \ln \left(\frac{3\pi\Delta}{2} (\Delta + \sqrt{1+\Delta^2}) + \frac{3\pi-4}{2} \right) \right].$$

Asymptotically $I(\Delta) = I_1(\Delta) + I_2(\Delta)$ is linear,

$$I(\Delta) \simeq \Delta + \left(1 - \frac{3}{\pi}\right) \Delta^{-1} + O[\Delta^{-3} \ln(\Delta)]. \quad (3.13)$$

Although the coefficient of $1/\Delta$ is small, yet higher order corrections are expected to reduce it to the near zero value found in Eq. (2.21).

IV. ANGULAR DOMINANCE ANALYTIC SOLUTION

For large E^2 and small radial excitation, Δ is small as can be seen from Eq. (2.18). Since for a massless quark the leading classical Regge trajectory corresponds to circular motion and in that case $\Delta=0$ and we are in the ultra-relativistic regime $v_{\perp} \approx 1$. In this section we examine the behavior of

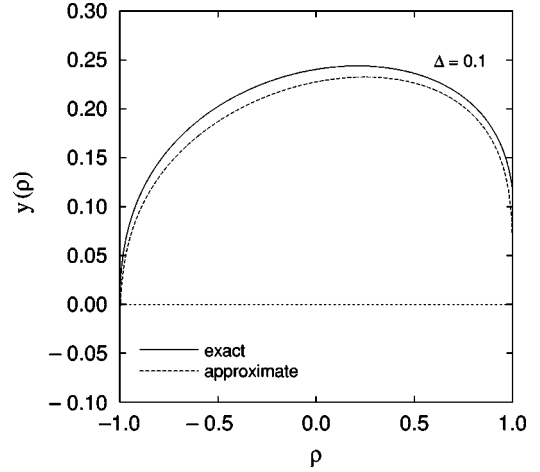


FIG. 6. A comparison of the exact numerical solution for $y(\rho) = (1 - v_{\perp}^2)^{1/2}$ from Eq. (2.13) and the solution of the cubic approximation, Eq. (4.2), for $\Delta = 0.1$.

Eqs. (2.12) and (2.13) as v_{\perp} approaches unity.

The appropriate expansion parameter in this case is

$$y = \sqrt{1 - v_{\perp}^2} = \frac{1}{\gamma_{\perp}}, \quad (4.1)$$

which would be the radial velocity with a massless quark since a massless quark must have $v^2 = \dot{r}^2 + v_{\perp}^2 = 1$.

Our first task is to expand Eq. (2.12) for small y and Δ , which is an expansion about circular orbits. The result is

$$\frac{8}{3\pi} y^3 - \rho\Delta y^2 - (1 - \rho^2)\Delta^2 = 0. \quad (4.2)$$

The cubic term is critical. Without it, there would be no real solutions for $\rho^2 < 1$. Going to quartic order in y makes only minor changes. To demonstrate the accuracy of this approximation, we show in Fig. 6 the solution $y(\rho)$ of Eq. (4.2) and the exact result obtained by solving the original (exact) Eq. (2.12) for the value $\Delta = 0.1$.

For small Δ the $y(\rho)$ solution becomes more symmetric about $\rho = 0$. The approximate solution to the cubic equation (4.2) for small Δ is

$$y(\rho) \simeq \left(\frac{3\pi}{8}\right)^{1/3} (1 - \rho^2)^{1/3} \Delta^{2/3} + \frac{\pi}{8} \rho\Delta + \dots \quad (4.3)$$

By substitution of Eq. (4.3), we see that Eq. (4.2) is satisfied up to the two leading powers of Δ . As Δ becomes small the asymmetric term becomes of less relative importance and we may keep only the leading term in Eq. (4.3):

$$y(\rho) \rightarrow \left(\frac{3\pi}{8}\right)^{1/3} (1 - \rho^2)^{1/3} \Delta^{2/3}. \quad (4.4)$$

For $\Delta \ll 1$ and $y \ll 1$, the expression (2.13) for w reduces to

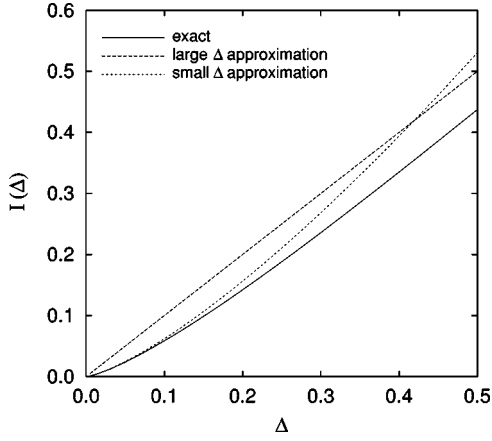


FIG. 7. A comparison of the exact numerical solution for $I(\Delta)$ (solid line) and the small Δ approximation (dotted line) and the large Δ approximation (dashed line).

$$w \simeq \frac{2}{\pi} y^2 \simeq \frac{1}{2} \left(\frac{3}{\pi} \right)^{2/3} (1 - \rho^2)^{2/3} \Delta^{4/3}. \quad (4.5)$$

With this approximation for w , the semiclassical quantization integral (2.17) becomes

$$I = \frac{4}{\pi} \int_{-1}^{+1} d\rho w(\rho) = \frac{8}{21} \left(\frac{3}{\pi} \right)^{5/6} \frac{\Gamma\left(\frac{2}{3}\right)}{\Gamma\left(\frac{7}{6}\right)} \Delta^{4/3}. \quad (4.6)$$

Numerically, we find

$$I(\Delta) \simeq 1.3367 \Delta^{4/3}. \quad (4.7)$$

In Fig. 7 we show the small Δ values of $I(\Delta)$. At small Δ we observe a distinct deviation from the linearity observed at larger Δ (see Fig. 2). The dotted curve shown in Fig. 7 is the small Δ leading term approximation of Eq. (4.7) and the dashed curve is the large Δ approximation to $I(\Delta)$. Although the small Δ analytic approximation clearly is converging to the correct numerical result for $\Delta \rightarrow 0$, deviations from the exact $I(\Delta)$ are evident around $\Delta = 0.3$. For $\Delta > 0.4$, the large Δ approximation to $I(\Delta)$ is better.

V. CONCLUSION

We have argued in Sec. I that the straight string model of confinement is accurate for ordinary hadron dynamics and that it is therefore a serious candidate for long-range QCD. Semiclassical quantization of the straight string agrees well with a fully quantized calculation [3], as shown in Fig. 3. The semiclassical method allows considerable analytic insight into string confinement in hadrons. In particular, when one or two of the quarks are massless, the entire spectroscopy is generated by a single integral function $I(\Delta)$ given in Eq. (2.17). For almost all accessible states $I(\Delta) \simeq \Delta$ which, by Eq. (2.18), immediately gives the simple pattern of Eq. (1.1), as illustrated in Fig. 8. Since even low-lying meson

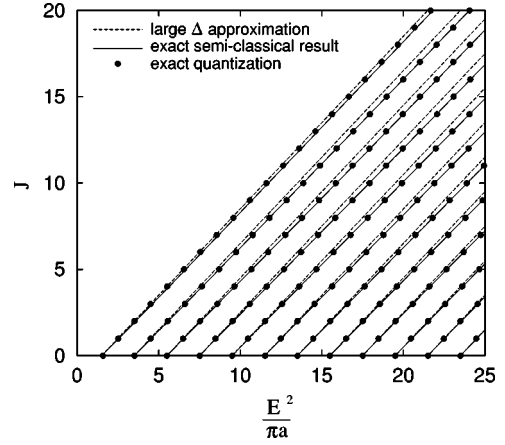


FIG. 8. The Regge trajectories from the large Δ approximation (dashed lines) of Eq. (1.1) in comparison to the exact numerical semiclassical analysis (lines) and the results of numerical canonical quantization (dots).

dynamics is dominated by the confining region, the observation of degenerate towers of mesons of the same parity becomes a key prediction of QCD.

The deviations from the simple pattern (1.1) are small and come when $\Delta < 1$. For observed meson states this corresponds to large angular momentum and small radial excitation. That is, deviations from (1.1) occur for mesons lying near the “leading” Regge trajectory. We showed in Sec. IV that $I(\Delta)$ is proportional to $\Delta^{4/3}$ for $\Delta \ll 1$ and the analytic approximation agrees well with the exact numerical $I(\Delta)$, as can be seen in Fig. 7.

To make the above statement more explicit we show in Fig. 8 a recreation of Fig. 3 but now adding a dashed line representing the analytic result (3.5) which becomes exact for large n and small J . For large J and small n the Regge trajectories seem to have a slightly smaller slope. In Fig. 9 we show the Δ values in this orbital dominant regime and we see that Δ is less than 1. As seen in Fig. 7, $I(\Delta) < \Delta$ and this reduction accounts for the difference between the dashed and solid (exact) curves in Fig. 8.

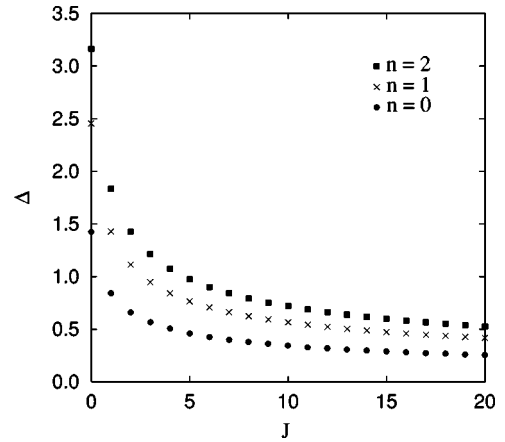


FIG. 9. The dependence of Δ upon the angular momentum quantum number J and the radial quantum number n . Increasing J leads to decreasing Δ .

A final observation is that $I(\Delta) \rightarrow \Delta$ follows from the radially dominant regime and not from the nearly circular approximation. This limit automatically gives straight, evenly spaced Regge trajectories.

ACKNOWLEDGMENT

This work was supported in part by the U.S. Department of Energy under Contract No. DE-FG02-95ER40896.

-
- [1] Y. Nambu, in *Symmetries and Quark Models*, edited by R. Chand (Gordon and Breach, New York, 1970); T. Goto, *Prog. Theor. Phys.* **46**, 1560 (1971); L. Susskind, *Nuovo Cimento A* **69**, 457 (1970); A. M. Polyakov, *Phys. Lett.* **103B**, 207 (1981).
- [2] A. Chodos and C. B. Thomas, *Nucl. Phys.* **B72**, 509 (1974); I. Bars, *ibid.* **B111**, 413 (1974); I. Bars and A. Hanson, *Phys. Rev. D* **13**, 1744 (1976); K. Kikkawa and M. Sato, *Phys. Rev. Lett.* **38**, 1309 (1977); M. Ida, *Prog. Theor. Phys.* **59**, 1661 (1978); K. Johnson and C. Nohl, *Phys. Rev. D* **19**, 291 (1979).
- [3] D. LaCourse and M. G. Olsson, *Phys. Rev. D* **39**, 2751 (1989); C. Olson, M. G. Olsson, and K. Williams, *ibid.* **45**, 4307 (1992); M. G. Olsson and K. Williams, *ibid.* **48**, 417 (1993); M. G. Olsson and S. Veseli, *ibid.* **51**, 3578 (1995); M. G. Olsson, S. Veseli, and K. Williams, *ibid.* **53**, 4006 (1996).
- [4] T. J. Allen, M. G. Olsson, and S. Veseli, *Phys. Lett. B* **434**, 110 (1998).
- [5] C. Olson, M. G. Olsson, and K. Williams, *Phys. Rev. D* **45**, 4307 (1992).
- [6] N. Brambilla and B. M. Prospero, *Phys. Lett. B* **236**, 69 (1990); G. S. Bali and P. Boyle, *Phys. Rev. D* **59**, 114504 (1999).
- [7] A. Yu. Dubin, A. B. Kaidalov, and Yu. A. Simonov, *Phys. Lett. B* **323**, 41 (1994); *Yad. Fiz.* **56**, 213 (1993); V. L. Morgunov, A. V. Nefediev, and Yu. A. Simonov, *Phys. Lett. B* **459**, 653 (1999).
- [8] T. J. Allen, M. G. Olsson, and S. Veseli, *Phys. Rev. D* **59**, 094011 (1999); **60**, 074026 (1999).
- [9] R. E. Langer, *Phys. Rev.* **51**, 669 (1937); M. S. Child, *Molecular Collision Theory* (Academic, New York, 1974).
- [10] T. J. Allen, M. G. Olsson, and S. Veseli, *Phys. Rev. D* **62**, 094021 (2000).